ACS NANO

Cite This: ACS Nano 2018, 12, 378−384

www.acsnano.org

ARTICLE

Efficient Steplike Carrier Multiplication in Percolative Networks of Epitaxially Connected PbSe Nanocrystals

Aditya Kulkarni,[†] Wiel H. Evers,[†] Stanko Tomić,[‡] Matthew C. Beard,[§] Daniel Vanmaekelbergh,[∥] and Laurens D. A. Siebbeles*[,†]

[†]Optoelectronic Materials Section, Department of Chemical Engineering, Delft University of Technology, Van der Maasweg 9, 2629 HZ Delft, The Netherlands

[‡]Joule Physics Laboratory, School of Computing, Science and Engineering, University of Salford, Manchester M5 4WT, United Kingdom

[§]National Renewable Energy Laboratory (NREL), Golden, Colorado 80401, United States

[∥]Debye Institute for Nanomaterials Science, University of Utrecht, Princetonplein 1, 3584 CC Utrecht, The Netherlands

Supporting Information

ABSTRACT: **Carrier multiplication (CM) is a process in which a single photon excites two or more electrons. CM is of interest to enhance the efficiency of a solar cell. Until now, CM in thin films and solar cells of semiconductor nanocrystals (NCs) has been found at photon energies well above the minimum required energy of twice the band gap. The high threshold of CM strongly limits the benefits for solar cell applications. We show that CM is more efficient in a percolative network of directly connected PbSe NCs. The CM threshold is at twice the band gap and increases in a steplike fashion with photon energy. A lower CM efficiency is found for a solid of weaker coupled NCs. This demonstrates that the coupling between NCs strongly affects the CM efficiency. According to device simulations, the measured CM efficiency would significantly enhance the power conversion efficiency of a solar cell.**

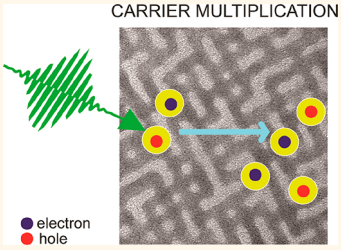

KEYWORDS: *nanocrystal networks, carrier multiplication, charge carrier mobility, terahertz spectroscopy, solar cell efficiency*

Photoexcitation of an electron in a semiconductor produces an electron−hole (e−h) pair with excess energy equal to the difference of the photon energy and the band gap. The electron and hole can release their excess energy in the form of heat *via* phonon emission. A charge with excess energy greater than the band gap can also relax by exciting another electron across the band gap. This process of carrier multiplication (CM) leads to generation of multiple e−h pairs per absorbed photon. CM is of great interest to enhance the photocurrent produced in a photovoltaic device.[1−6] In this context, lead chalcogenide nanomaterials have received particular attention because their band gap can be tuned to values near 1 eV, which is optimal for exploitation of CM in solar cells. The occurrence of CM has been observed in lead chalcogenide quantum dots in dispersion[7−9] and thin film solids,[6,10,11] nanorods,[2,12−14] nanosheets,[15] and bulk.[16]

For device applications, the charges produced *via* CM must be sufficiently mobile to prevent Auger recombination and to enable their extraction at external electrodes. Charge mobilities in the range of 1−40 $cm^2\ V^{-1}\ s^{-1}$ have been found for thin film solids of PbSe nanocrystals (NCs) that are connected by short organic ligands.[11,17,18] Interestingly, a PbSe NC solid with 1,2-ethanediamine ligands has shown a lower threshold for CM than for the same NCs in dispersion.[8,11] In this PbSe NC solid, the NCs are to some extent also coupled directly by thin atomic necks.[19] Hence, electronic coupling appears not only to be beneficial to charge mobility but also to reduce the threshold energy of CM. The coupling has been further enhanced by facet-specific oriented attachment of NCs.[20−23] In the latter case, further thermal annealing of the formed superlattice results in the formation of a percolative PbSe network, in which the NCs are connected *via* strong crystalline bridges in the in-plane directions. There are, on average, less than four connections per nanocrystal in this system. The percolative network can hence be considered as a planar system with a dimensionality between 2 and 1 with straight segments in orthogonal directions (see Figure 1A). The short-range mobility of charge carriers was found to attain values as high as 260 $cm^2\ V^{-1}\ s^{-1}$ for a probing electric field oscillating in the terahertz (THz) frequency range.[23] Note that the mobility in bulk PbSe is a few times higher than this value. The low band

Received: September 13, 2017
Accepted: December 14, 2017
Published: December 14, 2017

DOI: 10.1021/acsnano.7b06511
ACS Nano 2018, 12, 378−384

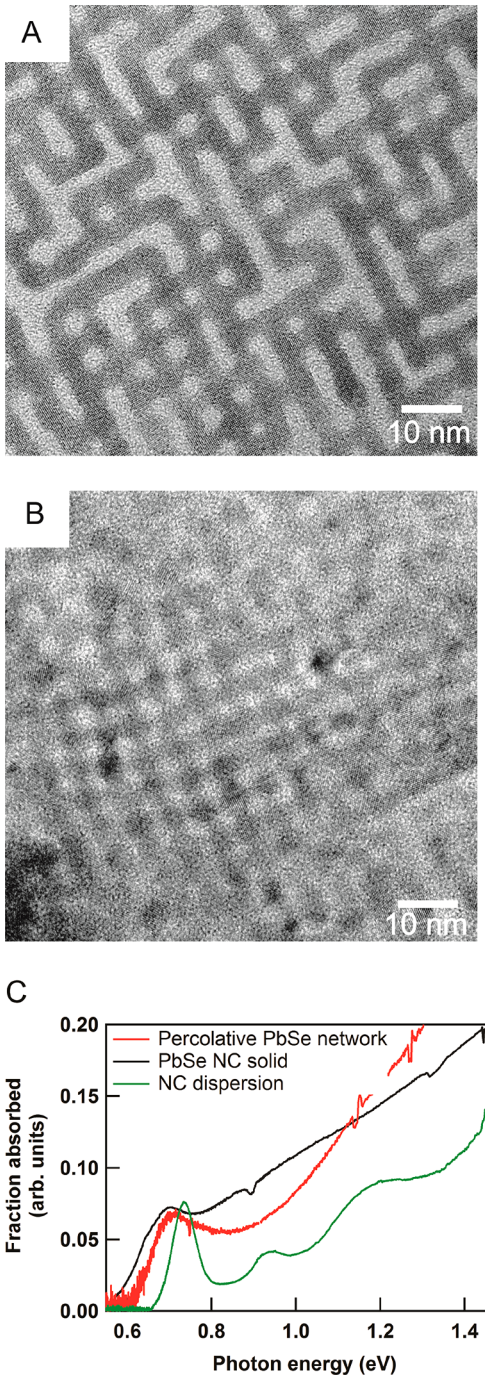

Figure 1. Structure and optical absorption. (A) TEM image of a monolayer percolative PbSe network (scale bar represents 10 nm). (B) TEM image of a NC solid (scale bar represents 10 nm). (C) Optical absorption spectra of a monolayer percolative PbSe network, the PbSe NC solid, and a NC dispersion in tetrachloroethylene.

gap of a bulk PbSe crystal makes it, however, unsuitable for solar cell applications.[3,4,16]

The aim of the current work is to determine to what extent the enhanced electronic coupling in percolative PbSe networks affects the CM threshold energy and efficiency in addition to the beneficial effect on charge mobility already reported in ref 23. We studied the quantum yield for charge carrier photogeneration in percolative PbSe networks and a PbSe NC solid, using optical-pump THz-probe (OPTP) time-domain spectroscopy. We found that CM in percolative PbSe networks has lower threshold energy and is more efficient than in films of PbSe NCs coupled by organic ligands.[11] Interestingly, the CM efficiency follows a steplike dependence on photon energy and reaches a value of about 1.4 at the minimum required photon energy of twice the band gap. According to detailed-balance calculations, the CM efficiency realized in the percolative PbSe network would enhance the power conversion efficiency of a solar cell by ~8% over the Shockley–Queisser limit for a band gap of 0.7 eV at 1 sun. The results have great promise for development of highly efficient third-generation solar cells.

RESULTS AND DISCUSSION

Structure and Optical Absorption of a Percolative PbSe Network and PbSe NC Solid. We studied CM in planar percolative PbSe networks with structure such as that shown in the transmission electron microscope (TEM) image of Figure 1A (see Methods). Such networks have a thickness of 5.8 nm, which is equal to the diameter of the NCs from which they were prepared.[20,23] Similar to our previous work, the center-to-center distance between the NCs in the plane of the network is 6.4 ± 0.1 nm. The NCs are connected by crystalline necks with a thickness of 4.0 ± 0.4 nm and an average of 2.6 ± 0.7 necks per NC.[23] The entire percolative system thus forms a planar single rocksalt PbSe crystal with the [100] crystal axes being the principal axes. The attached NCs form straight segments with average length of about 20 nm. For comparison, we also studied a thin film solid of PbSe NCs connected by 1,2-ethanediamine ligands with cubic ordering to some extent and relatively thin atomic necks between part of the NCs (see Methods).[19] The NC solid has a thickness of about 55 ± 10 nm corresponding to 10 layers of NCs. Figure 1B shows a TEM image of a NC solid. It exhibits relatively thin necks between part of the NCs, and it is more disordered than the percolative network. More details about the structure of such a NC solid can be found in refs 18 and 19.

Figure 1C shows that the optical absorption spectra of the percolative PbSe network, and the NC solid shows a broadened peak around 0.70 ± 0.01 eV. This peak is slightly red-shifted from the first excitonic transition of PbSe NCs dispersed in tetrachloroethylene (see Figure 1C). This can be attributed to the electronic coupling between NCs in the percolative network and the solid.[23] Photoluminescence from the percolative network and the NC solid could not be detected (see Methods), which implies that electrons and holes recombine predominantly nonradiatively. In what follows, we take the energy of the peak absorption maximum as the band gap of the material (*i.e.*, E_g = 0.70 eV). For the percolative network, the tail at the low-energy side is less broad than for the NC solid. This may be due to the more ordered structure of the network and the smaller number of connections to other NCs in the two-dimensional network, as compared to the NC solid (see Figure 1A,B).

THz Conductivity and Quantum Yield of Charge Carrier Photogeneration. Figure 2 shows THz conductivity signals, $S(t)$ (see Methods), for the percolative PbSe network and the NC solid after excitation with pump photon energies of 1.08 and 0.77 eV, respectively. These photon energies are below twice the band gap so that CM cannot occur. According to our previous studies, photoexcitation of these samples does not lead to a significant yield of neutral excitons, and therefore, the quantum yield of charge carriers can be considered equal to

DOI: 10.1021/acsnano.7b06511
ACS Nano 2018, 12, 378–384

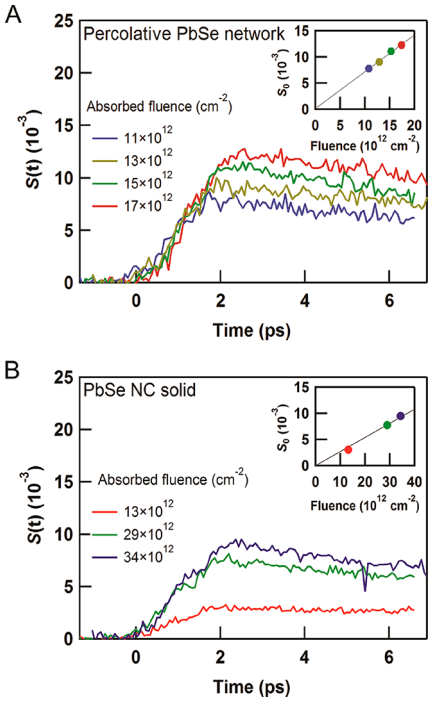

Figure 2. THz conductivity signal for different pump fluences. (A) THz conductivity signal induced by excitation of the percolative PbSe network at photon energy of 1.08 eV. (B) THz conductivity signal induced by excitation of the PbSe NC solid at photon energy 0.77 eV.

one (*i.e.*, ϕ = 1; see eqs 1 and 2 in Methods).[18,23] The THz conductivity signal is directly proportional to the sum of the time-dependent density of electrons and holes weighted by their mobility. The ~2 ps rise time of the THz conductivity signals in Figure 2 reflects the duration of the THz waveform. After the initial rise, $S(t)$ is merely constant up to 2.5 ps for all pump fluences, so that charge trapping or recombination is insignificant and the survival fractions of electrons and holes are equal to 1; that is, $f_e(t) = f_h(t) = 1$ for $t < 2.5$ ps; see eq 1 in Methods. In agreement with this, the initial THz conductivity signal S_0 (obtained by averaging $S(t)$ between 2.0 and 2.5 ps; see Methods) increases linearly with pump fluence; see the insets in Figure 2A,B. For up to at least 6 ps, the decay kinetics of the THz conductivity was found to be independent of pump photon energy, $h\nu$ (see Supplementary Figure S1), from which we infer that cooling of charge carriers from higher energy to the band edge is so fast that it does not affect the decay kinetics monitored in this experiment. This agrees with charge cooling times less than 2 ps reported for PbSe NCs before.[24,25] On a longer time scale on the order of 100 ps, the charges decay by trapping or recombination, as discussed before.[23]

The sum of the electron and hole mobilities, $\mu_e + \mu_h$, obtained from the data in Figure 2A for the percolative PbSe network is found to be 270 ± 10 cm^2 V^{-1} s^{-1}, which is close to previous results.[23] For the PbSe NC solid, the sum of the electron and hole mobilities obtained from the data in Figure 2B is 94 ± 4 cm^2 V^{-1} s^{-1}. This value is higher than that reported by Guglietta *et al.*,[17] which is due to the fact that we used a higher refractive index for PbSe (see Methods) and could in addition result from preparing the NC solid *via* layer-by-layer dip-coating rather than spin-coating. The larger electronic coupling due to the broad crystalline necks between the NCs in the percolative PbSe network causes the mobility to be higher than that in the NC solid, despite the smaller dimension of the network, between 2 and 1.

Determination of Carrier Multiplication Efficiency. The CM efficiency was determined from measurements of the initial THz conductivity signal S_0 for different pump photon energies, $h\nu$, as a function of pump fluence, N_a, analogous to the data in the insets in Figure 2. A similar approach has been used previously to determine the CM efficiency in PbS nanosheets and in bulk PbS and PbSe.[15,16] Figure 3A shows

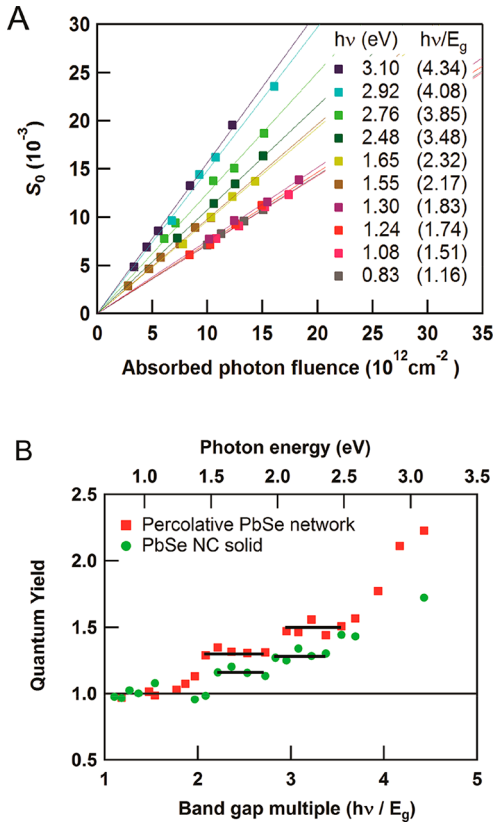

Figure 3. Initial THz conductivity and quantum yield for charge carrier photogeneration. (A) Initial THz conductivity of the percolative PbSe network *versus* absorbed pump fluence for photon energies as indicated. (B) Quantum yield as a function of band gap multiple ($h\nu/E_g$, bottom axis) and as a function of photon energy ($h\nu$, top axis) for the percolative PbSe network and the PbSe NC solid. The standard deviation in the quantum yields, as obtained from linear fits to experimental data as in panel A (and Supplementary Figure S2), is smaller than the data points.

that the slope of S_0 *versus* N_a for the percolative PbSe network is the same for photon energies up to 1.30 eV (*i.e.*, below $2E_g$ = 1.40 eV). This is to be expected because, at these energies, the quantum yield ϕ = 1. The slope exhibits increased values for photon energies of 1.55 eV and higher (*i.e.*, above $2E_g$), which is due to a higher quantum yield as a result of CM. We determine the slope corresponding with unity quantum yield by averaging the slopes in plots of S_0 *versus* N_a for photon energies less than twice the band gap. The quantum yield at higher photon energies is then obtained from the relative values of the slopes. The quantum yields for the percolative PbSe network and the PbSe NC solid were obtained from linear fits to the measured values of S_0 *versus* N_a, shown in Supplementary Figure S2. In Figure 3B, we show the quantum yield as a function of photon

DOI: 10.1021/acsnano.7b06511
ACS Nano 2018, 12, 378–384

energy, $h\nu$ (top axis), and as a function of photon energy normalized to the band gap, $h\nu/E_g$ (bottom axis).

Interestingly, Figure 3B shows that the onset of CM is near twice the band gap for both the percolative PbSe network and the PbSe NC solid. In addition, distinct steplike features appear in the quantum yield for the percolative network with plateaus at photon energies in the range of 1.5–2.0 eV ($2.1E_g - 2.9E_g$) and 2.0–2.6 eV ($2.9E_g - 3.7E_g$). At higher energies, the CM efficiency increases linearly. These characteristics of the CM efficiency were reproduced for a second percolative PbSe network (see Supplementary Figure S3). The PbSe NC solid exhibits a lower quantum yield with plateaus in the range of 1.5–1.9 eV and 2.0–2.4 eV.

Discussion of Carrier Multiplication Efficiency. Ideal staircase CM with the quantum yield increasing by one for each band gap multiple of the excess photon energy has been found for single-walled carbon nanotubes.[26] Such staircase behavior has also been reported for silicon nanocrystals embedded in a silicon dioxide matrix.[27] However, in the latter case, the nanocrystals were not coupled, preventing charge transport and solar cell applications. The percolative network and the NC solid of the present study combine steplike CM with onset at twice the band gap with high charge mobility.

For lead chalcogenide NCs in dispersion, the CM onset is at almost three times the band gap, and steplike features have not been reported.[9,14] Interestingly, the CM onset in lead chalcogenide nanorods is lower than that for NCs in dispersion, with the lowest reported threshold energy being $2.23E_g$.[12,14] Our percolative PbSe network is a planar crystal that can, somehow, be considered as a system of small NC rods of variable length (on average, several PbSe NCs long) oriented and connected in two orthogonal [100] directions (see Figure 1A). This appears to reduce the CM threshold energy to the absolute minimum of twice the band gap and leads to steplike features. CM at twice the band gap implies that the photon energy in excess of the band gap is fully converted into kinetic energy of one type of carrier only, either the photoexcited electron or the hole, as shown in the lower panel of Figure 4. The plateaus in the quantum yield *versus* photon energy in Figure 3 can be due to fast cooling of the electron (or hole) from higher energy in a series of electronic states to a lower state from which CM takes place prior to further cooling. The fact that the quantum yield does not increase up to 2.0 (see Figure 3) at photon energy of $2E_g$ can have different origins. First of all, it could be that not all photon absorption processes result in a fully asymmetric distribution of the photon energy; that is, they donate the excess energy to one type of charge carrier only. Possibly, part of the photons distribute their energy in excess of the band gap in a more symmetric way over the electron and the hole, as indicated in the upper panel of Figure 4. Second, thermal decay from the level of the CM precursor state might be at play. Interestingly, for PbS nanosheets, the CM threshold was found to be at a much higher band gap multiple[15] than for the percolative PbSe network of the present work. It appears that the continuous nanosheets behave more like the bulk crystal in which CM has a higher threshold energy due to restrictions imposed by conservation of crystal momentum of the electrons involved in CM. The weakening of the rock salt periodicity in three orthogonal directions in the structure of a percolative network can relax these restrictions in favor of CM.

Insight into the occurrence of asymmetric electronic excitations, as shown in the lower panel of Figure 4, can be

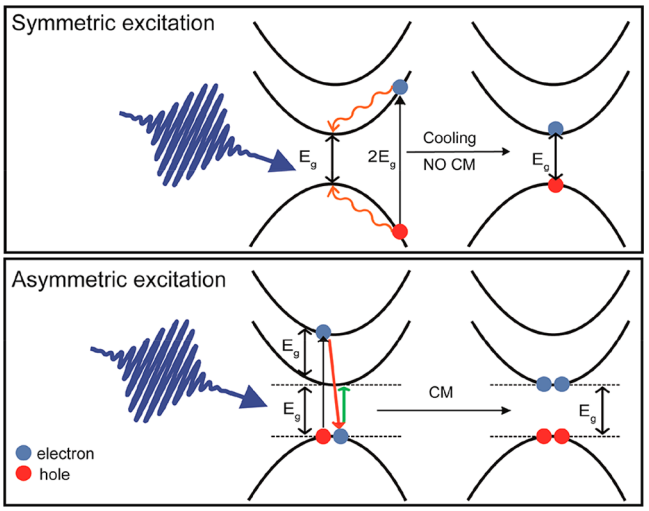

Figure 4. Photoexcitation and charge relaxation pathways. Upper panel: in a fully symmetric excitation at photon energy of twice the band gap, the excess energy is initially equally distributed between the electron (blue dot) and the hole (red dot), which subsequently relax by cooling to the band edges. Lower panel: in a fully asymmetric excitation, the excess photon energy can be transferred to excite another electron *via* CM. In the example of this figure, the electron in the second conduction band acquires the excess photon energy and subsequently relaxes *via* CM.

obtained from electronic structure calculations. To this end, we considered a percolative network of 12 × 12 coupled NCs taken from the TEM image in Figure 1A. Electronic states of this network were calculated using $k\cdot p$ theory with a basis set corresponding to the two highest valence band states and the two lowest conduction band states at the L-point in the first Brillouin zone of PbSe.[28,29] This four band model did not yield a significant amount of asymmetric electronic excitations. Apparently, the electronic states resulting from mixing of the four band-edge states in the percolative network are to a large extent still resembling the almost symmetric energy dispersion of the valence and conduction bands in bulk PbSe. Hence, the four band-edge states at the L-point are insufficient to describe asymmetric excitations. A next step would be to include states along the Σ-path in the first Brillouin zone or states at higher energy at the L-point.[25,30] It thus turns out that a proper description of CM in the percolative networks requires a more advanced theoretical approach, such as $k\cdot p$ theory, with more electronic bands or density functional theory with modern exchange/correlation functionals.

Enhancement of the Allowable Solar Cell Power Conversion Efficiency. Using the measured data in Figure 3B for the quantum yield *versus* band gap multiple, we calculated the power conversion efficiency (PCE) of a solar cell exposed to an AM1.5 solar spectrum using the detailied-balance approach.[31,32] All incident solar light at photon energy above the band gap was assumed to be absorbed. The results are shown in Figure 5, together with the Shockley–Queisser limit and the ideal staircase behavior of CM. The CM efficiency in the PbSe NC solid does not significantly enhance the maximum PCE as compared to the Shockley–Queisser limit. However, the CM efficiency measured for the percolative PbSe network would enhance the maximum allowable PCE from ~33% with no CM to ~37% for the percolative network, a net increase of 4% (red curve in Figure 5). At a fixed band gap, the increase in efficiency is greater. For a band gap of 0.7 eV, the PCE

DOI: 10.1021/acsnano.7b06511
ACS Nano 2018, 12, 378–384

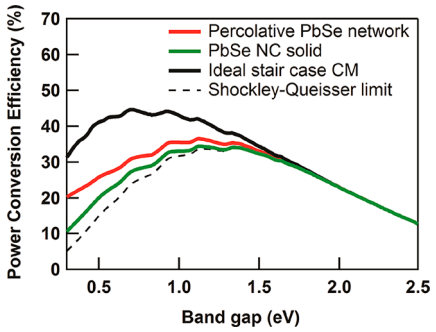

Figure 5. Simulated power conversion efficiency. Simulated power conversion efficiency of a solar cell exposed to an AM1.5 solar spectrum *versus* band gap for the percolative PbSe network and NC solid, together with the Shockley–Queisser limit and the ideal staircase behavior of CM. In the latter case, the quantum yield increases by one each time the photon energy increases by an amount equal to the band gap.

increases from 24% without CM to 32% for the measured CM in the percolative network, an increase of ∼8%. Under concentration, the PCE of all solar cells increases; however, when CM is present, the increase in PCE is much higher than that in the case of no CM.[3] At a concentration of 500×, the CM measured in the percolative network increases the PCE from 33 to 44% at 0.7 eV band gap.

Note that the optical absorption spectrum of the percolative network in Figure 1C shows a tail below the band gap. This will reduce the PCE with respect to the calculated values given above.[33] To fully exploit CM, the networks should be improved to achieve a more narrow tail.

CONCLUSIONS

In the percolative PbSe network, the threshold photon energy for CM to occur was found to be equal to the minimum value of twice the band gap. At the threshold, the quantum yield of charge carriers was found to increase to about 1.4 and to exhibit a plateau as a function of photon energy. At higher photon energy, the quantum yield exhibits a next steplike feature followed by a linear increase. Qualitatively similar results were obtained for a NC solid with organic ligands and thin atomic necks between part of the NCs. The PCE of a solar cell would be enhanced significantly by the CM efficiency found for the percolative PbSe network.

METHODS

Sample Preparation. All samples were prepared and stored in nitrogen atmosphere or under vacuum (for TEM) during measurements.

PbSe NCs with a diameter of 5.8 ± 0.4 nm passivated with oleic acid surface ligands were synthesized according to the method of Steckel *et al.*[34] Two-dimensional percolative PbSe networks were prepared by oriented attachment of the PbSe NCs, as described previously.[23] According to TEM measurements, the NCs are connected by necks with a thickness of 4.0 ± 0.4 nm with center-to-center distance of 6.4 ± 0.1 nm. The NC density in a network is 2.4 × 10^{12} cm^{-2}. To enhance the absorbed pump laser fluence and consequently the signal-to-noise ratio of the THz conductivity experiments, we stacked six monolayers of percolative PbSe networks on a quartz substrate, similar to our previous work.[23] The presence of long oleic acid ligands prevents electronic coupling between stacked layers. Consequently, charge transport only occurs within the layers and not from one layer to another. To get insight into the reproducibility of the experiments, we studied two percolative networks that were both prepared according to the procedure outlined above.

A PbSe NC solid was prepared *via* layer-by-layer dip-coating, using a DC multi-8 Nima Technology dip-coater.[11,18] At first, a quartz substrate was dipped into a dispersion of PbSe NCs with oleic acid ligands in hexane for 60 s. Subsequently, the sample was dipped into a 0.4 M solution of 1,2-ethanediamine ligands in methanol for 60 s for ligand exchange. Immediately after ligand exchange, the film was washed with methanol for 60 s. The above procedure was repeated 20 times to prepare a homogeneous film. The film has a thickness of 55 ± 10 nm, as determined with a Veeco Dektak 8 step profilometer.

TEM Characterization. TEM images and electron diffractograms were obtained using a Philips CM30T microscope operating at 200 kV.

Optical Characterization. Optical absorption spectra of the samples were measured using a PerkinElmer Lambda spectrophotometer equipped with an integrated sphere. Photoluminescence measurements were performed using a nanosecond pulsed pump–probe laser setup from Edinburgh Instruments (LP920) equipped with an InGaAs PIN photodiode detector G5853-23.

Terahertz Photoconductivity Measurements. Charge carriers were produced by excitation of the samples with optical pump pulses at varying wavelength, and the resulting photoconductivity was detected by time-domain THz spectroscopy,[35,36] analogous to our previous work.[23] Pump pulses were generated starting from a chirped-pulse amplified laser system (Mira-Libra, Coherent Inc.), which runs at 1.4 kHz and delivers pulses of 60 fs at 800 nm. Pump pulses (<100 fs) in the infrared and visible regions were obtained from optical parametric amplification seeded by white light (Topas-Coherent). A BaB_2O_4 (BBO) crystal was used to generate pump pulses at 400 nm. Single-cycle THz waveforms were generated by optical rectification in $LiNbO_3$ and detected in a ZnTe crystal by the electro-optic effect. A pinhole of 1.5 mm diameter was placed on the samples to ensure photoexcitation and probing of the same sample area during different experiments.

The photogeneration quantum yield of charge carriers, ϕ, and decay kinetics of charge carriers were obtained from the difference, $\Delta E(t_p,t) = E_{excited}(t_p,t) - E_0(t_p)$, of the maximum amplitude of the THz electric field at time t after the optical pump pulse, $E_{excited}(t_p,t)$, and the maximum amplitude of the THz waveform at time t_p after generation of the THz waveform, $E_0(t_p)$, in the absence of the pump pulse. The THz conductivity signal is then obtained according to[37,38]

$$S(t) = \frac{-\Delta E(t_p, t)}{E_0(t_p)} = \phi\left(\frac{f_e(t)\mu_e + f_h(t)\mu_h}{2c\varepsilon_0 n_{eff}}\right)N_a e \quad (1)$$

In eq 1, the functions $f_e(t)$ ($f_h(t)$) are the fractions of electrons (holes) that have survived from trapping or recombination, N_a is the absorbed pump photon fluence, c is the speed of light, ε_0 is the vacuum permittivity, n_{eff} is the effective refractive index in the THz frequency range, and e is the elementary charge. The value of n_{eff} was equal to 10.8, as inferred from the data in refs 23 and 39. The electron (hole) μ_e (μ_h) mobility in eq 1 is the real component due to the charge velocity in-phase with the THz field and averaged over the frequencies contained in the THz waveform (0.2–0.7 THz).

In our experiments, the THz conductivity signal $S(t)$ was found to reach a maximum value at a pump probe delay time near 2 ps (see Figure 2A) and to be merely constant up to 2.5 ps, so that $f_e(t)$ and $f_h(t)$ can be considered equal to unity on this time scale. To reduce the noise level, the quantum yield was obtained from $S(t)$ averaged over the time interval of 2.0–2.5 ps, which is denoted as the initial THz conductivity

$$S_0 = \phi A N_a \quad (2)$$

with $A = (\mu_e + \mu_h)e/2c\varepsilon_0 n_{eff}$. According to eq 2, the quantum yield of charge carriers, ϕ, can be obtained from the slope of a plot of S_0 *versus* N_a similar to previous studies.[15,16]

Note that studies of CM on NCs in suspensions have, in some cases, been affected by photocharging effects that could be avoided by stirring.[40] Such effects do not play any role in our measurements as we

DOI: 10.1021/acsnano.7b06511
ACS Nano 2018, 12, 378–384

determine the CM efficiency from the THz conductivity due to free mobile charges directly after the pump laser pulse. Hence, normalization to an optical signal at longer times that may be too small due to presence of trapped charges (and thus leads to overestimation of the quantum yield) does not play a role. Our samples were found to be stable during the THz conductivity measurements, and photodegrading did not occur.

ASSOCIATED CONTENT

Supporting Information

The Supporting Information is available free of charge on the ACS Publications website at DOI: 10.1021/acsnano.7b06511.

Figures S1−S3 (PDF)

AUTHOR INFORMATION

Corresponding Author

*E-mail: L.D.A.Siebbeles@tudelft.nl.

ORCID

Aditya Kulkarni: 0000-0002-5840-8768
Stanko Tomić: 0000-0003-3622-6960
Matthew C. Beard: 0000-0002-2711-1355
Daniel Vanmaekelbergh: 0000-0002-3535-8366
Laurens D. A. Siebbeles: 0000-0002-4812-7495

Author Contributions

A.K. and W.H.E. performed the spectroscopic experiments. A.K., W.H.E., and D.V. synthesized and structurally characterized the samples. A.K., W.H.E., and L.D.A.S. analyzed the experimental results. S.T. provided theoretical support. M.B. performed solar cell power conversion efficiency calculations. L.D.A.S. supervised the work and wrote the manuscript with A.K., W.H.E., M.B., and D.V. All authors discussed the results and commented on the manuscript.

Notes

The authors declare no competing financial interest.

ACKNOWLEDGMENTS

This work is part of the research programme of the Foundation for Fundamental Research on Matter (FOM), which is part of The Netherlands Organisation for Scientific Research (NWO), in the programme "Designing Dirac Carriers in Semiconductor Honeycomb Superlattices".

REFERENCES

(1) Beard, M. C.; Luther, J. M.; Semonin, O. E.; Nozik, A. J. Third Generation Photovoltaics Based on Multiple Exciton Generation in Quantum Confined Semiconductors. *Acc. Chem. Res.* **2013**, *46*, 1252−1260.

(2) Davis, N. J.; Bohm, M. L.; Tabachnyk, M.; Wisnivesky-Rocca-Rivarola, F.; Jellicoe, T. C.; Ducati, C.; Ehrler, B.; Greenham, N. C. Multiple-Exciton Generation in Lead Selenide Nanorod Solar Cells with External Quantum Efficiencies Exceeding 120%. *Nat. Commun.* **2015**, *6*, 8259.

(3) Hanna, M. C.; Beard, M. C.; Nozik, A. J. Effect of Solar Concentration on the Thermodynamic Power Conversion Efficiency of Quantum-Dot Solar Cells Exhibiting Multiple Exciton Generation. *J. Phys. Chem. Lett.* **2012**, *3*, 2857−2862.

(4) Nozik, A. J. Quantum Dot Solar Cells. *Phys. E* **2002**, *14*, 115−120.

(5) Semonin, O. E.; Luther, J. M.; Choi, S.; Chen, H. Y.; Gao, J.; Nozik, A. J.; Beard, M. C. Peak External Photocurrent Quantum Efficiency Exceeding 100% *via* MEG in a Quantum Dot Solar Cell. *Science* **2011**, *334*, 1530−1533.

(6) Ten Cate, S.; Sandeep, C. S.; Liu, Y.; Law, M.; Kinge, S.; Houtepen, A. J.; Schins, J. M.; Siebbeles, L. D. A. Generating Free Charges by Carrier Multiplication in Quantum Dots for Highly Efficient Photovoltaics. *Acc. Chem. Res.* **2015**, *48*, 174−181.

(7) Trinh, M. T.; Houtepen, A. J.; Schins, J. M.; Hanrath, T.; Piris, J.; Knulst, W.; Goossens, A. P.; Siebbeles, L. D. A. In Spite of Recent Doubts Carrier Multiplication Does Occur in PbSe Nanocrystals. *Nano Lett.* **2008**, *8*, 1713−1718.

(8) Ellingson, R. J.; Beard, M. C.; Johnson, J. C.; Yu, P.; Micic, O. I.; Nozik, A. J.; Shabaev, A.; Efros, A. L. Highly Efficient Multiple Exciton Generation in Colloidal PbSe and PbS Quantum Dots. *Nano Lett.* **2005**, *5*, 865−871.

(9) Smith, C.; Binks, D. Multiple Exciton Generation in Colloidal Nanocrystals. *Nanomaterials* **2014**, *4*, 19−45.

(10) Aerts, M.; Suchand Sandeep, C. S.; Gao, Y.; Savenije, T. J.; Schins, J. M.; Houtepen, A. J.; Kinge, S.; Siebbeles, L. D. A. Free Charges Produced by Carrier Multiplication in Strongly Coupled PbSe Quantum Dot Films. *Nano Lett.* **2011**, *11*, 4485−4489.

(11) Sandeep, C. S.; ten Cate, S.; Schins, J. M.; Savenije, T. J.; Liu, Y.; Law, M.; Kinge, S.; Houtepen, A. J.; Siebbeles, L. D. A. High Charge-Carrier Mobility Enables Exploitation of Carrier Multiplication in Quantum-Dot Films. *Nat. Commun.* **2013**, *4*, 2360.

(12) Cunningham, P. D.; Boercker, J. E.; Foos, E. E.; Lumb, M. P.; Smith, A. R.; Tischler, J. G.; Melinger, J. S. Enhanced Multiple Exciton Generation in Quasi-One-Dimensional Semiconductors. *Nano Lett.* **2011**, *11*, 3476−3481.

(13) Padilha, L. A.; Stewart, J. T.; Sandberg, R. L.; Bae, W. K.; Koh, W. K.; Pietryga, J. M.; Klimov, V. I. Aspect Ratio Dependence of Auger Recombination and Carrier Multiplication in PbSe Nanorods. *Nano Lett.* **2013**, *13*, 1092−1099.

(14) Padilha, L. A.; Stewart, J. T.; Sandberg, R. L.; Bae, W. K.; Koh, W. K.; Pietryga, J. M.; Klimov, V. I. Carrier Multiplication in Semiconductor Nanocrystals: Influence of Size, Shape, and Composition. *Acc. Chem. Res.* **2013**, *46*, 1261−1269.

(15) Aerts, M.; Bielewicz, T.; Klinke, C.; Grozema, F. C.; Houtepen, A. J.; Schins, J. M.; Siebbeles, L. D. A. Highly Efficient Carrier Multiplication in PbS Nanosheets. *Nat. Commun.* **2014**, *5*, 3789.

(16) Pijpers, J. J. H.; Ulbricht, R.; Tielrooij, K. J.; Osherov, A.; Golan, Y.; Delerue, C.; Allan, G.; Bonn, M. Assessment of Carrier-Multiplication Efficiency in Bulk PbSe and PbS. *Nat. Phys.* **2009**, *5*, 811−814.

(17) Guglietta, G. W.; Diroll, B. T.; Gaulding, E. A.; Fordham, J. L.; Li, S.; Murray, C. B.; Baxter, J. B. Lifetime, Mobility, and Diffusion of Photoexcited Carriers in Ligand-Exchanged Lead Selenide Nanocrystal Films Measured by Time-Resolved Terahertz Spectroscopy. *ACS Nano* **2015**, *9*, 1820−1828.

(18) Talgorn, E.; Gao, Y.; Aerts, M.; Kunneman, L. T.; Schins, J. M.; Savenije, T. J.; van Huis, M. A.; van der Zant, H. S.; Houtepen, A. J.; Siebbeles, L. D. A. Unity Quantum Yield of Photogenerated Charges and Band-Like Transport in Quantum-Dot Solids. *Nat. Nanotechnol.* **2011**, *6*, 733−739.

(19) Sandeep, C. S.; Azpiroz, J. M.; Evers, W. H.; Boehme, S. C.; Moreels, I.; Kinge, S.; Siebbeles, L. D. A.; Infante, I.; Houtepen, A. J. Epitaxially Connected PbSe Quantum-Dot Films: Controlled Neck Formation and Optoelectronic Properties. *ACS Nano* **2014**, *8*, 11499−11511.

(20) Evers, W. H.; Goris, B.; Bals, S.; Casavola, M.; de Graaf, J.; van Roij, R.; Dijkstra, M.; Vanmaekelbergh, D. Low-Dimensional Semiconductor Superlattices Formed by Geometric Control over Nanocrystal Attachment. *Nano Lett.* **2013**, *13*, 2317−2323.

(21) Geuchies, J. J.; van Overbeek, C.; Evers, W. H.; Goris, B.; de Backer, A.; Gantapara, A. P.; Rabouw, F. T.; Hilhorst, J.; Peters, J. L.; Konovalov, O.; Petukhov, A. V.; Dijkstra, M.; Siebbeles, L. D. A.; van Aert, S.; Bals, S.; Vanmaekelbergh, D. *In Situ* Study of the Formation Mechanism of Two-Dimensional Superlattices from PbSe Nanocrystals. *Nat. Mater.* **2016**, *15*, 1248−1254.

(22) Boneschanscher, M. P.; Evers, W. H.; Geuchies, J. J.; Altantzis, T.; Goris, B.; Rabouw, F. T.; van Rossum, S. A.; van der Zant, H. S.; Siebbeles, L. D. A.; Van Tendeloo, G.; Swart, I.; Hilhorst, J.; Petukhov,

A. V.; Bals, S.; Vanmaekelbergh, D. Long-Range Orientation and Atomic Attachment of Nanocrystals in 2D Honeycomb Superlattices. *Science* **2014**, *344*, 1377−1380.
(23) Evers, W. H.; Schins, J. M.; Aerts, M.; Kulkarni, A.; Capiod, P.; Berthe, M.; Grandidier, B.; Delerue, C.; van der Zant, H. S.; van Overbeek, C.; Peters, J. L.; Vanmaekelbergh, D.; Siebbeles, L. D. A. High Charge Mobility in Two-Dimensional Percolative Networks of PbSe Quantum Dots Connected by Atomic Bonds. *Nat. Commun.* **2015**, *6*, 8195.
(24) Spoor, F. C.; Kunneman, L. T.; Evers, W. H.; Renaud, N.; Grozema, F. C.; Houtepen, A. J.; Siebbeles, L. D. A. Hole Cooling Is Much Faster Than Electron Cooling in PbSe Quantum Dots. *ACS Nano* **2016**, *10*, 695−703.
(25) Spoor, F. C. M.; Tomic, S.; Houtepen, A. J.; Siebbeles, L. D. A. Broadband Cooling Spectra of Hot Electrons and Holes in PbSe Quantum Dots. *ACS Nano* **2017**, *11*, 6286−6294.
(26) Gabor, N. M.; Zhong, Z.; Bosnick, K.; Park, J.; McEuen, P. L. Extremely Efficient Multiple Electron-Hole Pair Generation in Carbon Nanotube Photodiodes. *Science* **2009**, *325*, 1367−1371.
(27) Timmerman, D.; Valenta, J.; Dohnalová, K.; de Boer, W. D. A. M.; Gregorkiewicz, T. Step-Like Enhancement of Luminescence Quantum Yield of Silicon Nanocrystals. *Nat. Nanotechnol.* **2011**, *6*, 710−713.
(28) Kang, I.; Wise, F. W. Electronic Structure and Optical Properties of PbS and PbSe Quantum Dots. *J. Opt. Soc. Am. B* **1997**, *14*, 1632−1646.
(29) Aeberhard, U.; Vaxenburg, R.; Lifshitz, E.; Tomic, S. Fluorescence of Colloidal PbSe/PbS QDs in NIR Luminescent Solar Concentrators. *Phys. Chem. Chem. Phys.* **2012**, *14*, 16223−16228.
(30) An, J. M.; Franceschetti, A.; Dudiy, S. V.; Zunger, A. The Peculiar Electronic Structure of PbSe Quantum Dots. *Nano Lett.* **2006**, *6*, 2728−2735.
(31) Beard, M. C.; Midgett, A. G.; Hanna, M. C.; Luther, J. M.; Hughes, B. K.; Nozik, A. J. Comparing Multiple Exciton Generation in Quantum Dots to Impact Ionization in Bulk Semiconductors: Implications for Enhancement of Solar Energy Conversion. *Nano Lett.* **2010**, *10*, 3019−3027.
(32) Hanna, M. C.; Nozik, A. J. Solar Conversion Efficiency of Photovoltaic and Photoelectrolysis Cells with Carrier Multiplication Absorbers. *J. Appl. Phys.* **2006**, *100*, 074510.
(33) Jean, J.; Mahony, T. S.; Bozyigit, D.; Sponseller, M.; Holovský, J.; Bawendi, M. G.; Bulović, V. Radiative Efficiency Limit with Band Tailing Exceeds 30% for Quantum Dot Solar Cells. *ACS Energy Lett.* **2017**, *2*, 2616−2624.
(34) Steckel, J. S.; Yen, B. K.; Oertel, D. C.; Bawendi, M. G. On the Mechanism of Lead Chalcogenide Nanocrystal Formation. *J. Am. Chem. Soc.* **2006**, *128*, 13032−13033.
(35) Ulbricht, R.; Hendry, E.; Shan, J.; Heinz, T. F.; Bonn, M. Carrier Dynamics in Semiconductors Studied with Time-Resolved Terahertz Spectroscopy. *Rev. Mod. Phys.* **2011**, *83*, 543−586.
(36) Lloyd-Hughes, J.; Jeon, T. I. A Review of the Terahertz Conductivity of Bulk and Nano-Materials. *J. Infrared, Millimeter, Terahertz Waves* **2012**, *33*, 871−925.
(37) Murphy, J. E.; Beard, M. C.; Nozik, A. J. Time-Resolved Photoconductivity of PbSe Nanocrystal Arrays. *J. Phys. Chem. B* **2006**, *110*, 25455−25461.
(38) Hendry, E.; Koeberg, M.; Schins, J. M.; Nienhuys, H. K.; Sundstrom, V.; Siebbeles, L. D. A.; Bonn, A. Interchain Effects in the Ultrafast Photophysics of a Semiconducting Polymer: THz Time-Domain Spectroscopy of Thin Films and Isolated Chains in Solution. *Phys. Rev. B: Condens. Matter Mater. Phys.* **2005**, *71*, 125201.
(39) Hyun, B. R.; Bartnik, A. C.; Koh, W. K.; Agladze, N. I.; Wrubel, J. P.; Sievers, A. J.; Murray, C. B.; Wise, F. W. Far-Infrared Absorption of PbSe Nanorods. *Nano Lett.* **2011**, *11*, 2786−2790.
(40) McGuire, J. A.; Sykora, M.; Joo, J.; Pietryga, J. M.; Klimov, V. I. Apparent *versus* True Carrier Multiplication Yields in Semiconductor Nanocrystals. *Nano Lett.* **2010**, *10*, 2049−2057.

DOI: 10.1021/acsnano.7b06511
ACS Nano 2018, 12, 378−384